CONDUCTION MECHANISMS IN LILLIE'S IRON-WIRE MODEL OF NERVE

LING Y. WEI *and* R. H. NEUMAN

From the Biophysical Research Laboratory, Electrical Engineering Department, University of Waterloo, Waterloo, Ontario, Canada

ABSTRACT Based on theory and experiment, we found that the conduction through the oxide film in Lillie's iron-wire model is dominated by Schottky emission at low fields (below 10^6 v/cm), by electron tunneling from trap to trap at intermediate fields and by direct tunneling (Fowler-Nordheim type) at higher fields (above 3×10^6 v/cm). The trap-to-trap tunneling is considered to give rise to the negative resistance and the fixed position of the current maximum as observed. Some of the nervelike properties of the Lillie's model are interpreted on this tunneling mechanism.

INTRODUCTION

In 1918, Lillie published his result on the iron-wire nerve model now bearing his name. In this model, an iron wire immersed in a strong nitric acid (60–70% concentration) was found to possess many nervelike properties. This behavior depends upon the presence of a thin surface film of a higher iron oxide under the influence of the nitric acid. This layer, so long as it is intact, is highly resistant and impermeable to the acid, and hence prevents the latter from reacting with the iron. The iron under the protection of the oxide film is said to be in a passive state. The wire can be activated by applying a negative potential to the iron and a positive potential to the acid. When the current density exceeds a certain threshold, the oxide film is reduced and breaks down and the exposed region becomes active. A local current then flows from this active region to the adjacent passive region and makes the latter active. The active region will be oxidized by the acid and soon returns to the passive state. The state of activity is thus automatically propagated over the whole length of the wire similar to nerve impulses. The iron-wire model has shown: (*a*) polar activation, (*b*) the all-or-none response, (c) the strength-duration relation, (*d*) refractoriness, i.e. it is unable to respond to a second stimulus if it follows the previous one within a certain interval, and (*e*) transmission of impulse wave. For over 50 years, Lillie's iron wire has stood as the best model which is capable of *physically* demonstrating a wide range of behavior of nerve axon.

Since the middle thirties, there have been numerous investigations of Lillie's model

from different standpoints (Bonhoeffer 1943, 1948, 1953; Yamagiwa, 1948, 1950 *a*, 1950 *b*; Frank, 1956; Tasaki and Bak, 1959; Frank and Fitzhugh, 1961; Suzuki, 1967). However, the physical mechanism for electric conduction in Lillie's model is still elusive. That this has not come about is largely due to the lack of knowledge in conduction through the thin oxide film which is in a solid form in spite of its aqueous environment. In the past ten years, there have been extensive studies of thin film conduction in solid-state physics. With this accumulated knowledge available, we are now able to reinvestigate Lillie's model from a new standpoint. Since the oxide film is the heart of the problem, we shall give a brief account of it here to facilitate the discussion later on.

From electrometric and X-ray diffraction experiments on iron in neutral solution, Nagayama and Cohen (1962, 1963) have concluded that the passive oxide consists of two layers: a layer of magnetite (Fe_3O_4) nearest the metal, and an outer layer of γ-ferric oxide (Fe_2O_3). Their electrometric measurements of the total equilibrium sheath thickness yielded values ranging from 10 to 30 A, depending on the anodic passivating potential.

In their model the γ-Fe_2O_3 layer is regarded as both the chemically protective and the electrically limiting layer. The inner Fe_3O_4 layer is simply assumed to be an electronic conductor. There is evidence that the outermost portion of the γ-Fe_2O_3 layer is further oxidized to a cation vacancy cubic oxide containing iron of a valency greater than three.

The ellipsometric measurements of Ord and De Smet (1966) have confirmed that the oxide in neutral solutions can attain thickness up to 40 A. Moreover, they lend further support to a two-layer model. Some of Ord's recent optical results have directly distinguished between the two oxide layers.[1] Typically the thickness of the inner Fe_3O_4 layer is at least twice as great as that of the outer γ-ferric oxide layer. Since the total sheath thickness is thought not to exceed 50 A, an upper limit for the thickness of the outer oxide layer would be about 16.7 A.

From the viewpoint of electrical conductivity, we have now a thin insulating film (Fe_2O_3) sitting between two conductors. To simulate the situation in nerve, the inner conductor (iron) is held negative in all of our experiments. We shall first present our experimental results and then elucidate the conduction mechanisms in the oxide film based on the existing theories. At the end, some discussion will be given on the nerve-like properties of Lillie's model to illustrate the implications of the tunneling mechanism.

EXPERIMENTAL

Methods

We have taken two kinds of measurements, one for dynamic characteristics and another for steady-state characteristics.

[1] Ord, J. L. 1969. Private conversations.

For dynamic measurements, an experimental setup similar to Tasaki and Bak's (1959) was used to apply a slowly varying triangular voltage across the oxide film. Fig. 1 shows the negative feedback voltage-clamp system which was employed for this purpose. In this circuit a Hewlett-Packard 3300A function generator (Hewett-Packard Co., Palo Alto, Calif.) yielded a triangular command potential V_c with a period of about 50 sec. The current through the film was always such as to make the voltage between iron and platinum almost equal to V_c.

Current and voltage were simultaneously displayed on a two-channel Tektronix oscilloscope, model 502A (Tektronix, Inc., Beaverton, Ore.). The helipot battery configuration merely served to shift the zero reference of the function generator output, so that the voltage applied to the iron was always zero or negative with respect to the platinum.

The iron sample consisted of a short piece of wire about 1 mm in diameter which was coated with beeswax. Only the tip of the wire was exposed to acid. Although the tip was initially sanded to about grit 600, repeated activations of the sample resulted in extreme surface roughness.

The distance between the iron surface and the platinum voltage-clamp electrode was generally 1 mm or less. This distance was mildly critical; it was found that after a number of activations when the iron surface had retreated up into its beeswax envelope, the N-shaped portion of the current-time curve became less pronounced.

There were two kinds of steady-state measurements in our study. Current through the oxide was measured as a function of temperature under conditions of constant voltage between platinum and iron. Voltage employed ranged from 0.1 to 0.75 v (iron negative). In most of the trials, 15.8 N (70%) acid was used. The acid was stirred vigorously in all cases. Temperature readings were obtained by a copper constantan thermocouple which was protected from acid by means of a glass tube containing a small amount of ethylene glycol solution. Readings were taken at 20-min intervals. The temperature was varied by means of a Tenney temperature controller (Tenney Engineering, Inc., Union, N. J.) over a range from about -27 to $+40$°C.

In the steady-state current-voltage measurements a high input resistance Keithley 601 electrometer (Keithley Instruments, Inc., Cleveland, Ohio) was employed to measure the potential between the saturated KCl calomel reference electrode and iron. The sample con-

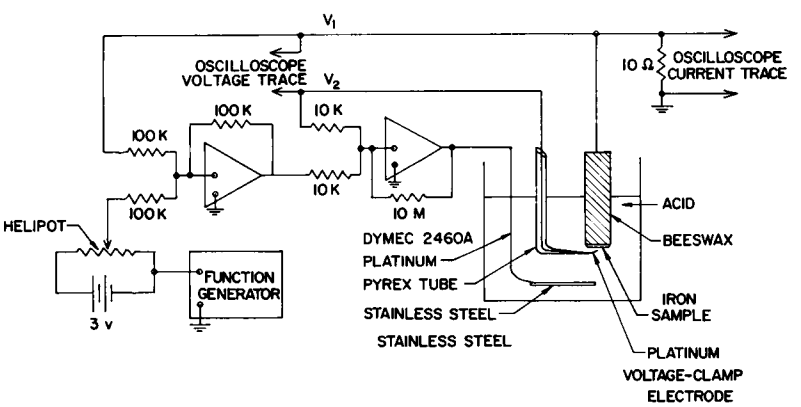

FIGURE 1 Voltage-clamp system for measuring the dynamic characteristic and also for measuring the steady-state characteristics with some modifications. K = kΩ, M = MΩ. Dymec 2460A operational amplifier (Hewett-Packard Co., Palto Alto, Calif.).

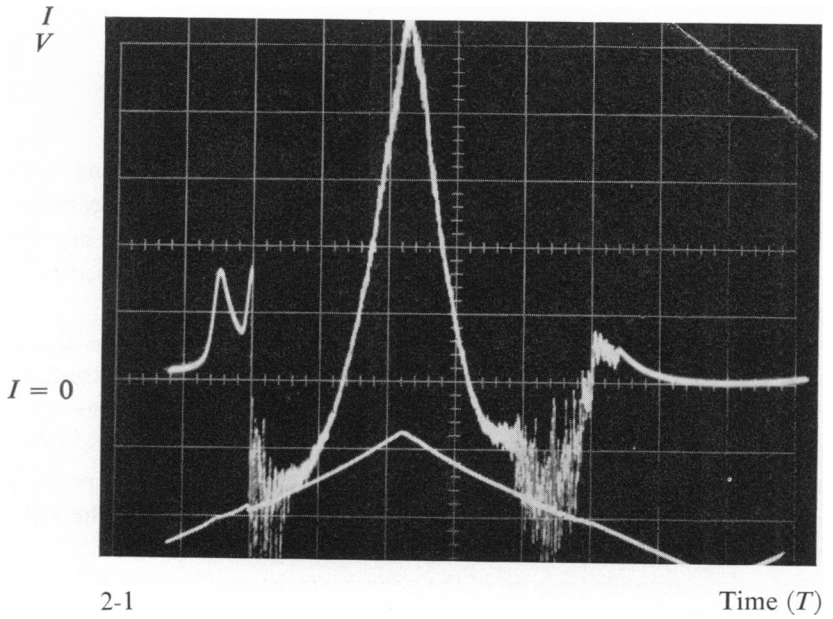

FIGURE 2 Dynamic current-voltage characteristic of γ-Fe_2O_3 oxide layer. I = 10 ma/cm, V = 0.5 v/cm, T = 5 sec/cm, 13 N HNO_3.

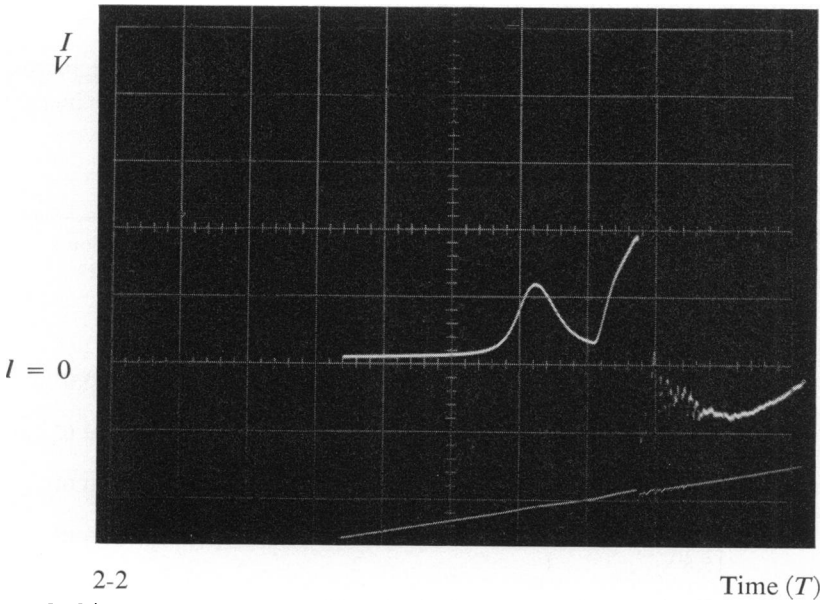

FIGURE 3 Time-expanded record of Fig. 2 showing more clearly the characteristic before the activation phase. I = 10 ma/cm, V = 0.5 v/cm, T = 2 sec/cm, 13 N HNO_3.

sisted of teflon-covered iron wire 1.3 mm in diameter with its tip exposed to acid. Stirred 13 N acid was used in all current-voltage experiments.

Results

Dynamic characteristics were obtained for acid concentrations ranging from 12 to 15.8 N. Typical curves are shown in Figs. 2 and 3. Zero voltage and current always correspond to grid lines in the photographs. The voltage trace usually does not quite reach zero because of the helipot-battery combination which was used to shift the zero reference of the generator output.

Fig. 2 shows a complete trace for iron in 13 N acid, and illustrates the negative incremental resistance region on the increasing voltage half-cycle. The sudden transition from passive to active state is manifested by a reversal in current due to the anodic chemical potential of bare iron in the acid. The instability in the current trace near transition points is due to a rapid succession of reduction and reoxidation of portions of the surface film. Repassivation is seen to occur when the voltage decreases to about 0.4 v.

Fig. 3 is a time-expanded record of the negative resistance region of Fig. 2. Results from these experiments are summarized in Table I. Numbers in line with numerical values for acid normality denote the number of trials which yielded a result. There appears to be a tendency for the negative resistance maxima and minima to occur at the same voltages, independent of the acid concentration. The only notable exceptions to this trend were the trials for 14 N acid concentration. This, however, could be attributed to relative flatness or lack of definition of most of the N-curves at this concentration.

From Table I it is apparent that as the acid concentrations were increased the cathodic potential necessary to activate the sheath also tended to increase. The

TABLE I

SUMMARY OF DYNAMIC CHARACTERISTICS

Acid concentration	Negative resistance maximum	Negative resistance minimum	Transition $P \rightarrow A^*$
	v	*v*	*v*
12 N	23 (trials)	21	26
	0.49 ± 0.03	0.53 ± 0.02	0.60 ± 0.03
13 N	6	9	11
	0.49 ± 0.02	0.54 ± 0.02	0.68 ± 0.03
13.5 N	3	6	6
	0.49 ± 0.01	0.54 ± 0.01	0.68 ± 0.01
14 N	5	11	10
	0.42 ± 0.03	0.50 ± 0.01	0.67 ± 0.03
15.8 N	1	2	2
	0.47	0.52 ± 0.04	0.71

*P—passive state, A—active state.

transitions from active to passive state were also found to occur at higher cathodic potentials. This was expected since the oxidizing power of the acid increases with concentration.

A detailed explanation of the dynamic characteristic will be given under "Theory."

The measured steady-state current-temperature characteristics are shown in Figs. 4 and 5. The slopes of these curves should yield the activation energies for conduction. It can be seen from the figures that activation energies varied widely from sample to sample, and often varied appreciably between successive trials for which the same sample was used. Over sixty trials, the activation energies were found to range from 0.1 to 1.0 ev.

There are two important facts to be noted from the current-temperature characteristics. First, there is a strong dependence of current on temperature. For example, in Fig. 4 the current varies over three decades in a temperature range of about 63°C. Second, the activation energy is seen to decrease with the applied voltage (field). The first fact implies that the conduction requires thermal activation particularly at low fields and the second fact indicates the lowering of barrier to conduction by the ap-

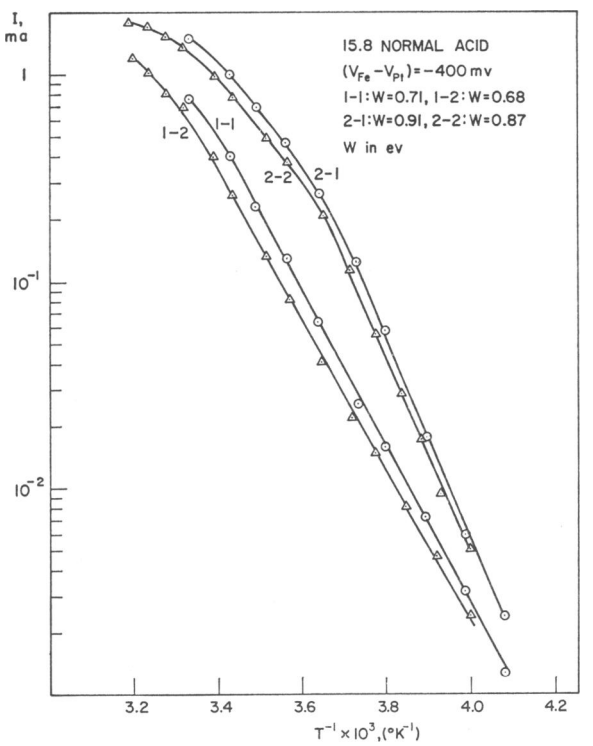

FIGURE 4 Oxide current-temperature characteristic at a bias voltage = −400 mv. W = activation energy = slope of the curve.

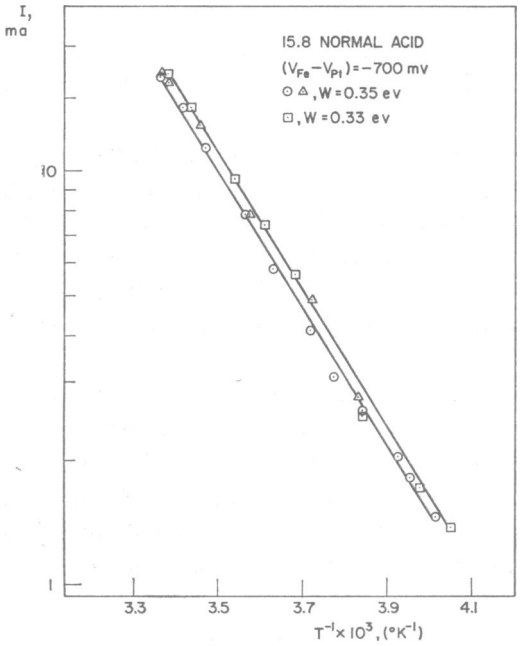

FIGURE 5 Oxide current-temperature characteristic at a bias voltage = —700 mv. W = activation energy = slope of the curve.

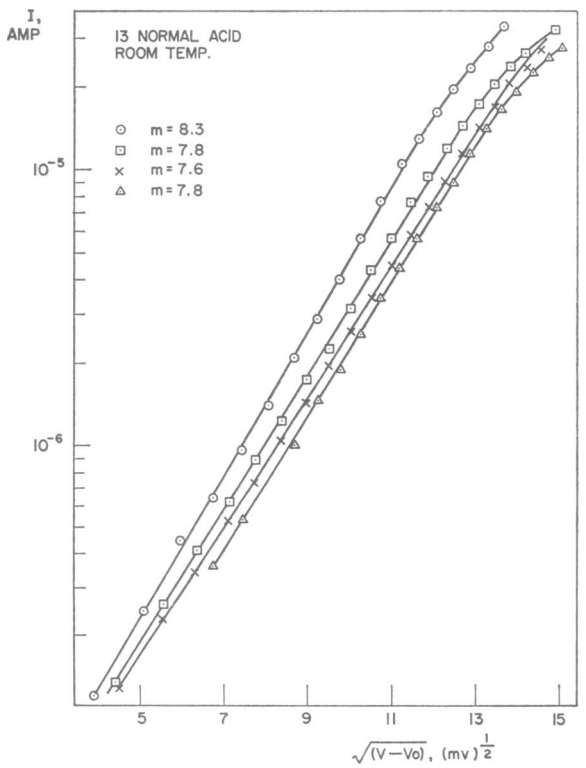

FIGURE 6 Steady-state oxide current-voltage characteristic (Schottky plot). m = slope of the curve.

plied field. These results are reasonable and can be understood when we come to "Theory."

The current-voltage behaviour of the oxide as shown in Fig. 6 can be described by

$$J = J_o \exp b \sqrt{V}, \tag{1}$$

which is characteristic of Schottky emission (1914). The Schottky emission is a thermionic emission over a surface barrier whose height is reduced by the image force and the applied field. Fig. 6 tends to indicate that at volts less than about 200 mv (or fields less than about 10^6 v/cm), the conduction is mainly controlled by the surface barrier. This will be discussed further in the next section.

THEORY

There are several mechanisms of electric conduction which could occur in thin insulating films (Lamb, 1967). Those which are relevant to our present study are: ionic conduction, Schottky emission, Poole-Frenkel emission, and tunneling. In ionic conduction, vacancies or ions jump over a potential barrier from one site to the next. The current density is given by

$$J = J_o \exp(-\phi/kT)(\exp[ZeFa/kT] - \exp[-ZeFa/kT]), \tag{2}$$

where ϕ is the barrier height, Z is the valency of the mobile carrier, F is the applied field; a is the distance between the two sites, k is the Boltzmann constant, and T is the absolute temperature.

Schottky and Poole-Frenkel emissions also exhibit an exponential dependence of current on inverse temperature. Electrode-limited Schottky emission from a metal consists of thermal activation of electrons over a barrier which has been lowered by classical coulombic image forces. In rationalized mks units, the current density is given by (Schottky, 1914)

$$J = \frac{4\pi mek^2(1 - R)T^2}{h^3} \exp\left(\frac{-\phi}{kT}\right) \exp\frac{(e^3/4\pi\epsilon)^{1/2}F^{1/2}}{kT}, \tag{3}$$

where h is Planck's constant, ϵ is the high frequency permittivity of the film, ϕ is the work function of the metal electrode, and R is a reflection parameter.

Poole-Frenkel emission is a bulk phenomenon consisting of field-enhanced thermal emission of electrons or holes from traps which are neutral when filled and charged when empty. Electron current is given by

$$J = e\mu N_o F \exp - \frac{\phi - (e^3/\pi\epsilon)^{1/2}F^{1/2}}{\gamma kT}, \tag{4}$$

where μ is electron mobility, ϕ is the energy difference between the emission site and

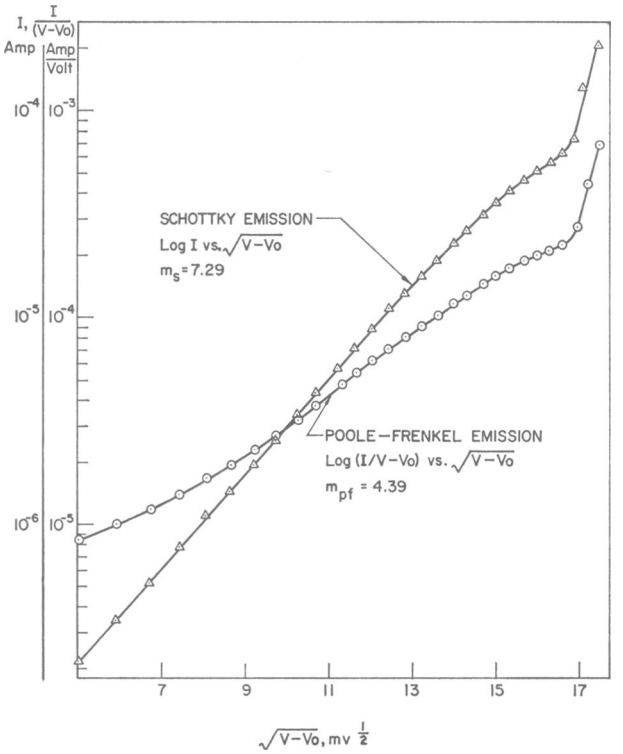

FIGURE 7 Comparison of Schottky and Poole-Frenkel plots for the same current-voltage data sample. m_s and m_{pf} designate the slopes of the two curves, respectively.

the bottom of the conduction band, N_o the effective electron density in the traps and conduction band of the oxide, and γ is a parameter which ranges from 1 to 2 depending on the position of the Fermi level.

For both ionic conduction (particularly at high fields) and Poole-Frenkel emission, a plot of log J vs. $(1/T)$ will yield a straight line with a slope proportional to the activation energy which is effective at the field strength used. For Schottky emission a plot of log (J/T^2) vs. $(1/T)$ will yield such a straight line. In our case, the temperature range was so limited that both log J and log (J/T^2) plots yielded straight lines with activation energies differing only in the second decimal place.

However, it is possible to discriminate between Poole-Frenkel emission and Schottky emission on the basis of experimental current-voltage data. Fig. 7, which displays the same set of data plotted in two ways, shows that the Schottky plot yields a very good straight line whereas the Poole-Frenkel plot displays a decided curvature at low voltage. Further evidence to favour Schottky emission and reject Poole-Frenkel emission is provided by the slopes of the two curves.

From equation 3, the slope of the Schottky plot, $\log_{10} J$ vs. $V_s^{1/2}$ should be

$$m_s = 0.435\, e^{3/2}(kT)^{-1}(4\pi\epsilon_o\epsilon' D)^{-1/2}. \quad (5)$$

Here it is assumed that the field within the oxide is uniform and equal to V_s/D where D is thickness of the current-limiting oxide layer. The ϵ' in equation 5 is the electronic or high frequency component of the dielectric constant and is given by

$$\epsilon' = n^2,$$

where n is the refractive index of the current-limiting oxide layer. From the recent experiment by Ord,[1]

$$\sqrt{\epsilon'} = n \simeq 2,$$

with this value substituted in equation 5, we obtain at room temperature,

$$m_s = (3.251 \times 10^{-4}) D^{-1/2}, \tag{6}$$

where D is in meters. The slopes of the curves in Fig. 6 are 7.6–8.3. Substituting these values into equation 6, we obtain values for D ranging from 15.4 to 18.3 A. These values are in excellent agreement with the value of 16.7 A, considered to be the maximum thickness for the outer γ-ferric oxide layer. On the other hand, the slope of the linear portion of the Poole-Frenkel plot in Fig. 7 is 4.39. Then from equation 4 and equation 6, which applies for $\gamma = 2$ in equation 4, the Poole-Frenkel plot yields a thickness value somewhere between 55 A (for $\gamma = 2$) and 220 A (for $\gamma = 1$). These values are considerably larger than 16.7 A for the γ-ferric oxide layer and thus make the Poole-Frenkel mechanism less likely than the Schottky mechanism.

It is somewhat difficult to make an unambiguous distinction between ionic conduction and Schottky emission on the basis of our data alone. If ionic conduction predominates, then from equation 2 a plot of log J against V should yield a straight line at high fields. The slope of this line is given by

$$m_i = 0.435 (e/kT) (a/D),$$

or at room temperature

$$a/D = 5.89 \times 10^{-2} m_i. \tag{7}$$

In Fig. 8 the same set of current-voltage data is plotted according to both ionic and Schottky emission relations. Although the Schottky plot yields a much better straight line, the downward curvature of the ionic plot in the low voltage region can be attributed to the second term in equation 2.

The factor a in equations 2 and 7 is the distance from a minimum to a maximum of the periodic barrier potential. This should be of the same order of magnitude as the lattice parameter, which is about 8.3 A according to Sewell, Stockbridge, and Cohen (1961). From Fig. 8 and equation 7, a/D is calculated to be 0.77. Assuming a value

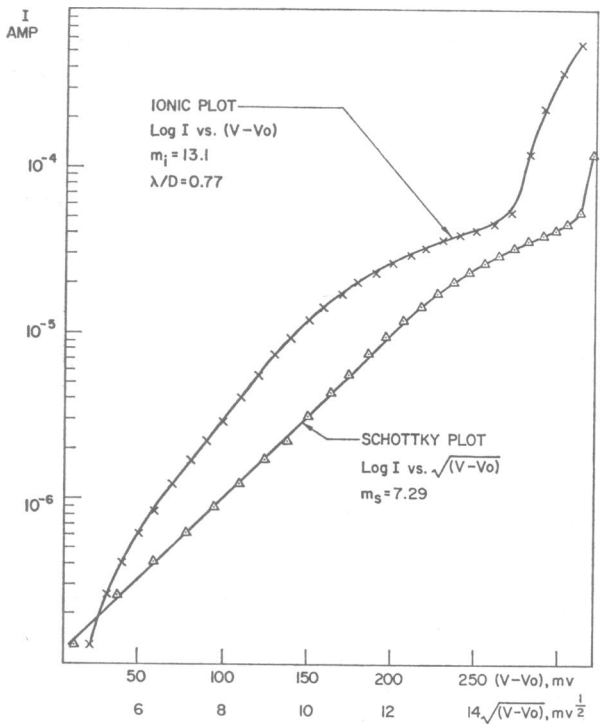

FIGURE 8 Comparison of Schottky and ionic plots for the same current-voltage data sample.

of 16.7 A for D, we obtain 12.8 A for a which is a little less than twice the value quoted in the above

Yet there are several reasons why ionic conduction is unlikely to occur. In all of our experiments the electric field was directed from the solution toward the iron, repelling positive ions towards the metal and negative ions toward the solution. Since oxygen ions are considerably larger than iron ions, ionic conduction would be primarily due to the migration of Fe^{2+} ions (which are negative with respect to the Fe^{3+} ions in the γ-Fe_2O_3 lattice) outward toward the solution.

In bulk ferric oxide, however, conduction arising from nonstoichiometric Fe^{2+} Fe^{4+} ions is primarily electronic. These ions act respectively as localized donors and acceptors, causing the exchange of slow electrons between themselves and neighboring Fe^{3+} ions over considerable activation barriers (Morin, 1958). This fact combined with the high mass of ions as compared with the effective mass of electrons, makes ionic conduction far less probable a mechanism than electronic conduction.

Experimentally, even in the regions of higher voltage, our data fitted Schottky emission somewhat better than they fitted ionic conduction. For example, in Fig. 8 significant departures from linearity begin to occur at 130 mv for the ionic plot whereas in the Schottky plot they do not set in until about 160 mv (or 10^6 v/cm).

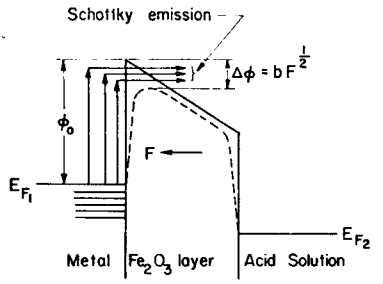

FIGURE 9 Energy diagram showing Schottky emission over a reduced surface barrier.

It is therefore concluded that until voltages approaching the negative region are attained (field greater than 10^6 v/cm), conduction proceeds primarily by Schottky emission of electrons into the conduction band of the oxide, as illustrated in Fig. 9.

In the dynamic characteristics of Figs. 2 and 3, we see that as the applied field exceeded 10^6 v/cm, the current increased to a maximum and then decreased to a minimum from where it rose sharply. The positions of current maxima and minima from Table I are rather fixed in a variety of conditions (acid concentrations and perhaps film thickness). It appears that some other mechanism than the ones previously discussed must play a dominant role at high fields in the oxide layer.

The one mechanism which we have mentioned but not discussed is electron tunneling. In a film of 20 A or so, quantum tunneling of electrons is quite possible. However, there are some structural factors which deserve our consideration. In the Fe_2O_3 layer, Fe^+, Fe^{2+}, and Fe^{4+} ions and perhaps some other defects would act as electron traps. In the energy band diagram, these traps are located in the energy gap below the bottom of the conduction band. Since the Fe_2O_3 layer is amorphous which has no periodic structure, and since the traps are distributed in random, the localized states will form a band within the energy gap. This is shown as L.S.B. in Fig. 10 *a*. In that diagram, ϕ_o (in volts) is the work function on the metal side, ϕ_c, the energy of the bottom of the conduction band of Fe_2O_3 above the Fermi level, and ϕ_i, the energy of the top of the localized states above the Fermi level.

Fig. 11 shows electron tunneling between trap states. Electrons are injected from the metal side below the Fermi level E_{F_1} into the nearest localized states of the Fe_2O_3 layer. They are trapped for a short while and then tunnel through a thin potential barrier (of width S) into the adjacent localized states. One notes that the height of each individual potential barrier is lowered by the field. For the case $V < \phi_i$ (see Fig. 10 *b*), the tunneling current is given by (Simmons and Verderber, 1967),

$$I = B \exp\left(-1.025s[\phi - \tfrac{1}{2}F_o\, d]^{1/2}\right) \sinh\left(0.128\delta s\, dV/[\phi - \tfrac{1}{2}F_o\, d]^{1/2}\right), \quad (8)$$

where s = the base width of each potential hill, d = the spacing between traps, F_o = the field at zero bias, ϕ = the level of injected electrons measured from the top of the surface barrier, and $\delta = (eN/\epsilon)^{1/2}$ with N = the density of localized states per unit energy and ϵ = the permittivity of the insulating film.

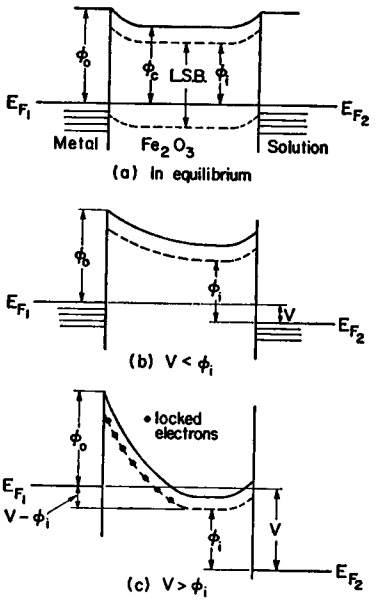

FIGURE 10 Energy band diagrams showing the role of the electron traps in the Fe_2O_3 layer in conduction: (*a*) at equilibrium, (*b*) bias voltage $V < \phi_i$, and (*c*) $V > \phi_i$. Note in-(*c*) black dots indicating the electrons "locked" in the localized states.

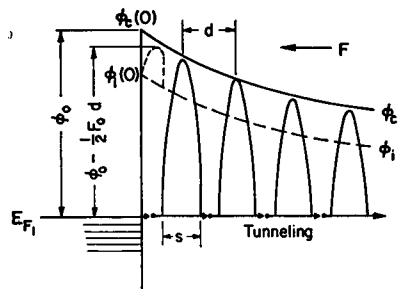

FIGURE 11 Electron tunneling between traps whose potentials are reduced by the field.

The above relation gives the tunneling current of electrons injected at a single level ϕ measured from the top of the surface barrier. The total tunneling current resulting from *all* the electrons injected will be

$$I(\infty) = \int_0^\infty I(\phi) f(\phi)\, d\phi, \tag{9}$$

where $f(\phi)$ is the Fermi function. The contribution is the greatest from the electrons injected at the Fermi level ϕ_o. Above ϕ_o, $f(\phi)$ falls off rapidly and below ϕ_o, $I(\phi)$ as seen from equation 8 drops sharply.

When the bias voltage V exceeds ϕ_i, electrons injected above ϕ_i will be "locked" in the localized states shown as black dots in Fig. 10 *c*. They are locked because they cannot see any other localized states at the same energy level into which they can tunnel. Tunneling umimpeded over the whole film thickness is possible only for elec-

trons injected below the ϕ_i level or at energies exceeding $\phi_o + V - \phi_i$ measured from the top of the surface barrier (see the left side of Fig. 10 *c*). The tunneling current is still given by equation 8 but with ϕ replaced by $\phi_o + V - \phi_i$. One can see immediately that $I(\phi_o + V - \phi_i)$ is an exponentially decreasing function of V and its peak value occurs when $V = \phi_i$ or when $\phi = \phi_o$. For the case of $V < \phi_i$, the tunneling current $I(\phi)$ is increasing with V and it reaches maximum when $V = \phi_i$ and $\phi = \phi_o$. $I(\phi_o)$ and $I(\phi_o + V = \phi_i)$ vs. V are plotted in Fig. 12. One sees now the rising and the falling parts of the *I-V* characteristic and a peak located at a constant $V = \phi_i$. The peak is sharp because we consider only the electrons injected from a "single" level. When tunneling electrons from *all* levels are taken into account, the peak will be rounded off. The dashed curve in Fig. 12 indicates the *total* tunneling current over a voltage range up to a value larger than ϕ_i. The resemblance of this curve to that shown in Fig. 3 is evident. From the above discussion, the negative resistance and the fixed position of current maxima observed in many cases can be understood based on the mechanism of tunneling from trap to trap in the Fe_2O_3 layer.

At larger bias voltages, the field in the Fe_2O_3 layer is so high that electrons can hardly be trapped. Under this condition, electrons would tunnel directly from one side to the other side of the insulating layer and the tunneling current is given by (Fowler and Nordheim, 1928)

$$I = CF^2 \exp(-b/F), \tag{10}$$

where F is the field and C and b are constants. This current rises very steeply with the field and it could be taken as the contribution following the current valley of the dynamic characteristic shown in Fig. 3.

The remaining question is, why tunneling is not as important as, or at least is masked by, Schottky emission at low fields? As can be seen from Fig. 10 *a*, at low fields, electrons injected from the metal at the Fermi level would mostly go to the deep traps. By deep traps we mean the traps which are located far down from the bottom of the conduction band. In general deep traps are much less numerous than shallow traps (close to the conduction band), and hence are far apart from one another. Since the tunneling probability decreases considerably with increasing distance, electrons in deep traps can hardly tunnel away. Furthermore, the attraction between an electron and a deep trap (for example, Fe^{4+}) is much greater than that between an electron and a shallow trap (for example, Fe^{+}). Thus an electron will become almost

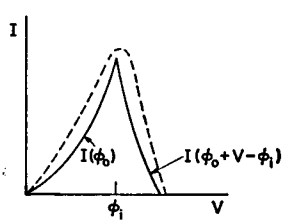

FIGURE 12 Solid curves for $I(\phi)$ and $I(\phi_o + V - \phi_i)$ vs. voltage as given by equation 8 with $\phi = \phi_o$ and $\phi_o + V - \phi_i$, respectively. Dashed curve is for the total tunneling current as given by equation 9.

completely immobilized once falling into a deep trap. So at low fields, tunneling of electrons from trap (deep) to trap is highly improbable. The only possible way to avoid trapping at low fields is that electrons in the metal are first thermally activated to the top of the surface barrier and then drift in the conduction band of the Fe_2O_3 layer. In this case, the rate of transport of electrons is mainly controlled by the height of the surface barrier which can be reduced by the image force and applied field. The conduction mechanism is then the Schottky emission. The experiment fully accords with this logic.

CONCLUSION

Based on theory and experiment, we can conclude that there are three conduction mechanisms in the Fe_2O_3 layer of Lillie's iron wire model: Schottky emission at low fields, tunneling from trap to trap at moderate fields, and direct tunneling from one side to the other side of the layer at high fields. It is the trap-to-trap tunneling which gives rise to negative resistance of the film. More clearly, the negative resistance stems from the fact that some electrons become locked in the localized state and thus unable to tunnel as the bias voltage exceeds a certain value at which the current reaches the peak.

With the above understanding in the conduction mechanisms, we may look at the nervelike properties of Lillie's iron-wire model from a fresh viewpoint. Since unattenuated impulse transmission requires in the wire a negative resistance which comes into being only for applied voltage exceeding ϕ_i, so $V = \phi_i$ is the threshold for the all-or-none response. In the trap-to-trap tunneling, an electron will spend some time (τ) in each trap and hence takes a certain length of time, say t_o crossing the whole Fe_2O_3 layer. If the duration of the stimulus is less than t_o, the foremost running electrons will either become trapped indefinitely or tunnel in random directions before reaching the other end due to the removal of the applied field and hence the wire will not be excited. The time an electron spends in each trap depends on the field; the higher the field, the shorter the trapping time (τ), and so the crossing time t_o. In other words, a greater strength of the stimulus requires a less duration to excite the wire. This agrees qualitatively with the strength-duration relation in nerve excitation.

As discussed previously, if the stimulating strength V exceeds ϕ_i, some electrons injected will be *locked* in the localized states (black dots in Fig. 10 *c*). These locked electrons can only diffuse away after the cessation of the stimulus and it will take some time before their complete withdrawal. If a second stimulus comes sooner, the injected electrons will find *filled* traps on their way and thus become jammed in the traffic. Hence the response to the second stimulus is either lost or largely subsided. This is equivalent to refractoriness in nerve and the time for the complete withdrawal of the locked electrons to the "absolute refractory period."

Conduction in thin films has become a very important subject in microelectronics and solid-state physics. That it finds its way to Lillie's iron-wire model and even offers

some plausible interpretations of the model's nervelike properties is highly interesting and stimulating. Perhaps in the area of nerve studies, the time has come for us to think more about its physics than about its biology.

We wish to thank Professor J. D. Ord for giving us much information about the iron oxide layer, and to acknowledge help from Dr. V. Joshi in the early stage of this experiment.

The work was supported by the National Research Council of Canada under Grant No. A 1252.

Received for publication 26 February 1970.

REFERENCES

BONHOEFFER, K. F. 1943. *Naturwissenschaften.* **31**:270.
BONHOEFFER, K. F. 1948. *J. Gen. Physiol.* **32**:69.
BONHOEFFER, K. F. 1953. *Naturwissenschaften.* **40**:301.
FOWLER, R. H., and L. NORDHEIM. 1928. *Proc. Roy. Soc. London.* **119A**:173.
FRANK, U. F. 1956. *Progr. Biophys. Biophy. Chem.* **6**:171.
FRANK, U. F., and R. FITZHUGH. 1961. *Z. Elektrochem.* **65**:156.
LAMB, D. R. 1967. Electrical Conduction Mechanisms in Thin Insulating Films. Methuen & Co. Ltd., London.
LILLIE, R. S. 1918. *Science (Washington).* **48**:51.
MORIN, E. J. 1958. *Bell. Syst. Tech. J.* **37**:1047.
NAGAYAMA, M., and M. COHEN. 1962. J. Electrochem. Soc. **109**:781.
NAGAYAMA, M., and M. COHEN. 1963. J. Electrochem. Soc. **110**:670.
ORD, J. L., and D. J. DESMET. 1966. J. Electrochem. Soc. **113**:1258.
SCHOTTKY, W. 1914. *Z. Phys.* **15**:872.
SEWELL, P. B., C. D. STOCKBRIDGE, and M. COHEN. 1961. J. Electrochem. Soc. **108**:933.
SIMMONS, J. G., and R. R. VERDERBER. 1967. *Proc. Roy. Soc. Ser. A. Math. Phys. Sci.* **301**:77.
SUZUKI, R. 1967. I.E.E.E. (*Inst. Elec. Electron. Eng.*) Trans. *Bio-Med. Eng.* **14**:114.
TASAKI, I., and A. F. BAK. 1959. *J. Gen. Physiol.* **42**:899.
YAMAGIWA, K. 1948. *Jap. Med. J.* **1**:557.
YAMAGIWA, K. 1950 *a. Jap. Med. J.* **1**:40.
YAMAGIWA, K. 1950 *b. Jap. J. Physiol.* **1**:48.